Journal of Functional Materials and Applied Engineering

Research Paper

Preparation and Protein Adsorption Properties of HEMA Modified PDMSPES Composite Membranes for ECMO Oxygenation Applications

Antonio Siegenfeld[1], Yaneer Maclay[2,*]

[1] IFISC (CSIC-UIB), Campus Universitat Illes Balears, 07071, Palma de Mallorca, Spain
[2] Departamento de Economía, Universidad Carlos III, Spain
*Corresponding author: Asiege066@hotmail.es (Antonio Siegenfeld); ymkeer@eco.uc3m.es (Yaneer Maclay)

Abstract. The clinical efficacy of extracorporeal membrane oxygenation (ECMO) remains severely limited by thrombogenesis and inflammatory responses induced by insufficient hemocompatibility of commercial oxygenation membranes. Herein, we report a facile surface engineering strategy to construct a hydrophilic HEMA-PDMS/PES composite membrane with balanced gas transport performance and antifouling properties. An amphiphilic HEMA-PDMS copolymer was first synthesized via free radical copolymerization, where the grafting density of hydroxyethyl methacrylate (HEMA) was precisely controlled to avoid compromising the intrinsic gas permeability of polydimethylsiloxane (PDMS). The copolymer was then coated on a porous polyethersulfone (PES) substrate fabricated by phase inversion, forming a dense, defect-free functional layer. Systematic characterization confirmed that the composite membrane maintained excellent thermal stability (no mass loss below 400 °C) and achieved a moderate surface water contact angle of ~40°, endowing it with both CO2/O2selectivity (α=6.53) and ultralow hemolysis rate (0.207%–0.434%). Protein adsorption assays demonstrated that HEMA modification reduced the maximum bovine serum albumin (BSA) adsorption capacity by up to 13.494% compared to unmodified PDMS/PES membranes. Combined Langmuir isotherm and pseudo-second-order kinetic fitting revealed that adsorption was dominated by chemisorption via hydrogen bonding between BSA polar residues and HEMA hydroxyl groups, while competitive hydration and hydrophobic interactions jointly modulated the adsorption behavior. This work not only clarifies the protein adsorption mechanism on amphiphilic silicone-based surfaces, but also provides a scalable material design paradigm for next-generation ECMO devices with extended safe operation duration.

Keywords: *hydroxyethyl methacrylate; polydimethylsiloxane; protein adsorption; hydrophilic modification; chemisorption; ECMO; hemocompatibility*

Received on 10 Apr 2022, Accepted on 15 June 2022, Published on 08 July 2022

1 Introduction

Extracorporeal membrane oxygenation has evolved into a critical life-sustaining intervention for individuals experiencing intractable cardiopulmonary compromise, encompassing acute respiratory distress syndrome, cardiogenic shock, and complications arising from cardiac surgical procedures [1,2]. As the core component of ECMO systems, the oxygenator membrane facilitates gas exchange by enabling CO_2 removal and O_2 uptake from venous blood outside the body, effectively assuming the function of native lungs [3]. Nevertheless, clinical outcomes of ECMO intervention remain constrained by thrombotic adverse events, affecting 10%–30% of recipients and elevating morbidity, mortality, and mechanical failure incidence [2,4]. Thrombotic cascade initiation commences with non-specific plasma protein adsorption (e.g., albumin, fibrinogen, immunoglobulins) onto the membrane surface upon hemocompatibility contact, subsequently activating platelet recruitment, activation, and fibrin clot propagation [5,6]. Thus, improving the hemocompatibility of oxygenator membranes by reducing protein adsorption is critical for enhancing ECMO performance and patient outcomes.

Polydimethylsiloxane (PDMS) has been widely used as an oxygenator membrane material since the 1980s due to its exceptional gas permeability (O_2 permeability ~800 Barrer), excellent thermal stability, and inherent physiological inertness [7,8]. However, the intrinsic hydrophobicity of PDMS (water contact angle ~110°)

promotes unfavorable interactions with blood components: hydrophobic surfaces induce conformational changes in adsorbed proteins, expose binding sites for platelets, and activate the coagulation cascade [9,10]. Surface modification of PDMS to enhance hydrophilicity represents a promising strategy to mitigate these issues, as hydrophilic surfaces reduce protein adsorption by forming a hydration layer that sterically hinders protein-membrane interactions [11].

Among various hydrophilic modifiers, hydroxyethyl methacrylate (HEMA) has gained significant attention due to its biocompatibility, ease of polymerization, and abundance of polar hydroxyl groups that promote surface hydration [12,13]. Previous studies have demonstrated that grafting HEMA onto PDMS via copolymerization yields amphiphilic HEMA-PDMS copolymers, which combine the gas permeability of PDMS with the hydrophilicity of HEMA [14,15]. Membranes fabricated from HEMA-PDMS exhibit reduced surface free energy, smoother morphology, and lower protein adsorption compared to pristine PDMS [16]. However, the underlying mechanism of protein adsorption on HEMA-PDMS surfaces—particularly the role of hydrogen bonding between HEMA polar groups and protein functional moieties—remains poorly understood. Additionally, the impact of HEMA modification on the gas separation performance (critical for oxygenator function) and hemocompatibility of PDMS-based composite membranes requires systematic investigation.

In this study, we aimed to (1) synthesize HEMA-PDMS copolymers via free radical copolymerization and fabricate HEMA-PDMS/PES composite membranes with a porous PES support; (2) characterize the physicochemical properties, gas permeation performance, and hemocompatibility of the composite membranes; (3) elucidate the kinetics, thermodynamics, and mechanism of BSA adsorption on HEMA-PDMS surfaces; and (4) provide theoretical insights for designing next-generation oxygenator membranes with enhanced hemocompatibility. Our results demonstrate that HEMA modification effectively reduces protein adsorption and hemolysis while maintaining favorable gas selectivity, offering a viable pathway for improving ECMO membrane performance.

2. Experimental Section

2.1 Materials

PDMS (RBG-0614, number-average molecular weight M = 5500) was supplied by Shandong Dongyue Chemical Co., Ltd. (China). Polyethersulfone (M = 30,000), hydroxyethyl methacrylate, azobisisobutyronitrile, and N,N′-methylenebisacrylamide were procured from Shanghai Aladdin Biochemical Technology Co., Ltd. (China). Polyethylene glycol (M = 1000) was obtained from Beijing Solarbio Science & Technology Co., Ltd. (China). Tetraethyl orthosilicate (98 wt%), bovine serum albumin, and sodium dodecyl sulfate (2 wt% solution) were supplied by Yancheng Saibao Biotechnology Co., Ltd. (China). N,N-Dimethylformamide, isooctane, and dibutyltin dilaurate were sourced from Tianjin Damao Chemical Reagent Factory (China). Phosphate-buffered saline (pH 7.2–7.4), heparinized New Zealand rabbit whole blood, and normal saline (0.9 wt% NaCl) were purchased from Shanghai Macklin Biochemical Co., Ltd. (China). All chemicals were of analytical grade and employed without additional purification unless otherwise stated.

2.2 Membrane Fabrication

2.2.1 Preparation of Porous PES Substrate Membranes

Polyethersulfone particulates were desiccated under vacuum at 120 °C for 12 h to eliminate residual moisture content. A casting solution was prepared by dissolving 15 wt% PES and 5 wt% PEG (porogen) in DMF under continuous stirring at 60 °C for 6 h, followed by ultrasonication (100 W) for 30 min and degassing at room temperature for 2 h to eliminate air bubbles. The PES support layer was manufactured through phase inversion methodology. The dope solution was cast onto a pristine glass substrate using a laboratory film applicator set to 25 μm thickness, then immediately quenched in a deionized water coagulation medium maintained at 25 °C for 30 min to induce phase separation. The resultant microporous membrane was exhaustively rinsed with deionized water to eliminate residual solvent and pore-forming agents, then preserved in fresh deionized water at 4 °C pending subsequent utilization.

2.2.2 Synthesis of HEMA-PDMS Copolymer

HEMA-PDMS copolymers were fabricated through free radical copolymerization. In a representative protocol, 0.9 g PDMS was solubilized in 130 mL isooctane under inert nitrogen atmosphere, then transferred to a three-necked round-bottom flask fitted with a reflux condenser. After purging with nitrogen for 5 min to exclude oxygen, 0.0103 g of AIBN (1 wt% relative to HEMA mass, initiator) and 0.0145 g of MBA (1.5 wt% relative to HEMA mass, crosslinking agent) were added. HEMA was then introduced dropwise at a PDMS:HEMA-PDMS copolymers were fabricated through free radical copolymerization. In a representative protocol, 0.9 g PDMS was solubilized in 130 mL isooctane under inert nitrogen atmosphere, then transferred to a three-necked round-bottom flask fitted with a reflux condenser. The HEMA monomer was introduced at a HEMA-to-PDMS mass ratio of 1.0:0.9, and the reaction mixture was thermally elevated to 85 °C under continuous agitation for 5 h. Following thermal quenching to ambient temperature, the crude product was precipitated in excess ethanol, isolated by filtration, and vacuum-desiccated at 40 °C for 24 h to afford the purified HEMA-PDMS copolymer. Copolymers with varying solid contents (2, 4, and 6 wt%) were prepared by adjusting the initial PDMS mass (1.8, 3.6, and 5.4 g) while maintaining the PDMS:HEMA mass ratio. For comparison, pristine PDMS solutions (2, 4, and 6 wt%) were prepared without HEMA, AIBN, or MBA.

2.2.3 Fabrication of HEMA-PDMS/PES Composite Membranes

A coating solution was prepared by adding TEOS (crosslinker) and DBTDL (catalyst) to the HEMA-PDMS solution at a mass ratio of HEMA-PDMS:TEOS:DBTDL = 25:10:1 under gentle stirring, followed by ultrasonication for 15 min to remove air bubbles. A pre-wetted PES substrate was immersed vertically into the coating solution for 2–3 s, ensuring complete wetting without trapped air bubbles. The coated membrane was withdrawn slowly, air-dried for 5 min, and cured in an oven at 85 °C for 2 h to complete crosslinking (Figure 1). The resulting composite membranes were designated as *x*H-P/P, where *x*denotes the HEMA-PDMS solid content (1, 2, 4, or 6 wt%). Unmodified PDMS/PES composite membranes (*x*P/P) were fabricated using identical procedures but with pristine PDMS coating solutions.

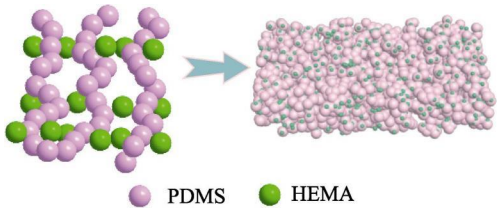

Figure 1 Schematic diagram of structure of HEMA-PDMS

2.3 Characterization Techniques

2.3.1 Morphological and Chemical Characterization

Membrane surface and cross-sectional architectures were characterized using a Nova Nano SEM 450 field emission scanning electron microscope (FEI, USA) operated at 5 kV accelerating potential. Specimens were cryogenically fractured in liquid nitrogen, metallized with gold via sputter coating prior to examination, and imaged under low-voltage secondary electron detection mode. Fourier-transform infrared spectra were acquired on a Nicolet iS50 spectrometer (Thermo Fisher Scientific, USA) spanning 4000–500 cm^{-1} at 4 cm^{-1} resolution with 32 accumulated scans per specimen. Thermogravimetric characterization was conducted on a Q50 analyzer (TA Instruments, USA) under nitrogen purge, with thermal ramping from 25 to 900 °C at 10 °C/min heating rate. Surface hydrophilicity was evaluated by measuring the static water contact angle (WCA) using a SL200KB goniometer (Kino, USA) at ambient temperature; five random locations per sample were measured, and the average value was reported.

2.3.2 Gas Permeation Performance

Gas permeation properties were tested using a custom-built apparatus as described previously [7]. Circular membrane specimens (1 cm diameter) were installed in a stainless-steel permeation cell. The upstream

compartment was pressurized to 0.1 MPa gauge using either pure CO_2 or O_2, while the downstream side remained at ambient pressure. The permeate flow rate was measured using a soap bubble flowmeter, and gas permeability (J, GPU; 1 GPU = 10^{-6} cm^3(STP)/(cm^2·s·cmHg)) was calculated using Equation (1):

$$J=(273.15+\theta)\times A\times t\times(\Delta p\times 76)273.15\times 0.1\times\Delta V \quad (1)$$

where ΔVis the volume of permeate gas (cm^3), θis the test temperature (25 °C), Ais the effective membrane area (cm^2), tis the permeation time (s), and Δpis the transmembrane pressure (MPa). Gas selectivity (α) for CO_2 over O_2 was calculated as the ratio of CO_2 permeability to O_2 permeability (Equation 2):

$$\alpha=JO2 \quad JCO2 \quad (2)$$

2.3.3 Hemocompatibility Evaluation

Hemolysis assays were conducted following ISO 10993-2017 guidelines to assess erythrocyte compatibility. Positive controls were prepared by diluting 10 mL of heparinized rabbit whole blood with 60 mL of deionized water (complete hemolysis), while negative controls consisted of 10 mL of blood diluted with 60 mL of normal saline (minimal hemolysis). Membrane specimens (1 cm diameter) underwent sequential pre-conditioning in normal saline and phosphate-buffered saline at 37 °C for 48 h each, followed by immersion in 5 mL positive control solution and incubation at 37 °C for 2 h. The treated samples were then centrifuged at 3000 rpm for 10 min, and the absorbance of the resulting supernatant was quantified at 545 nm using an X-3 UV-Vis spectrophotometer (Shanghai Yuanxi Instrument Co., Ltd., China). The hemolysis rate (HR, %) was calculated using Equation (3):

$$HR/\%=Dpc \quad -Dnc \quad Dt \quad -Dnc \quad \times 100 \quad (3)$$

where Dt is the absorbance of the sample, Dnc is the absorbance of the negative control, and Dpc is the absorbance of the positive control. All tests were performed in triplicate, and HR values <5% were considered acceptable for biomedical applications.

2.3.4 Protein Adsorption Studies

Bovine serum albumin, serving as a surrogate protein with comparable molecular dimensions and Stokes radius to human serum albumin, was employed to assess protein adsorption behavior [17,18]. Membrane specimens (1 cm diameter) underwent surface equilibration through sequential immersion in normal saline (37 °C, 48 h) and phosphate-buffered saline (37 °C, 48 h). For equilibrium adsorption isotherms, samples were immersed in 3 mL of BSA solutions with varying concentrations (500, 750, 1000, 1250, 1500 μg/mL) at 37 °C for 2 h. For adsorption kinetics, samples were incubated in 3 mL of 1 g/L BSA solution at 37 °C, and adsorption was terminated at predetermined time intervals (0.5, 1, 2, 4, 8, 12, 24, 48 h). For temperature-dependent studies, samples were incubated in 1 g/L BSA at 27, 32, 37, 42, and 47 °C for 2 h. Following incubation, membrane specimens were gently washed with fresh phosphate-buffered saline to eliminate weakly associated proteins, then immersed in 3 mL of 2% sodium dodecyl sulfate solution and agitated for 30 min to achieve complete BSA desorption. The BSA concentration in the desorption solution was determined by UV-Vis spectroscopy at 280 nm using a pre-established calibration curve: $y=0.00061x-0.00314$($R^2=0.99888$), where yis absorbance and xis BSA concentration (μg/mL). The equilibrium BSA adsorption capacity (q, μg/cm^2) was calculated using Equation (4):

$$q=S\rho V \quad (4)$$

where ρis the BSA concentration in the desorption solution (μg/mL), Vis the volume of the desorption solution (mL), and Sis the effective membrane surface area (cm^2).

2.4 Adsorption Modeling

2.4.1 Adsorption Isotherms

The Langmuir isotherm model, which assumes monolayer adsorption on a homogeneous surface with uniform binding energies, was used to fit equilibrium adsorption data (Equation 5):

q1 =qm ρKa 1 +qm 1 (5)

where qis the equilibrium adsorption capacity (μg/cm²), ρis the equilibrium BSA concentration in solution (μg/mL), qm is the maximum monolayer adsorption capacity (μg/cm²), and Ka is the adsorption equilibrium constant (mL/μg). Linear regression of 1/qvs. 1/ρyielded qm and Ka .

2.4.2 Adsorption Kinetics

Three kinetic models were employed to analyze adsorption dynamics:

Pseudo-first-order model: Assumes physisorption with a rate proportional to the number of available adsorption sites (Equation 6):

qt =qe (1−e−k1 t)(6)

Pseudo-second-order model: Describes chemisorption involving valence forces between adsorbent and adsorbate (Equation 7):

qt =1+k2 qe tk2 qe2 t (7)

Elovich model: Applicable to heterogeneous adsorption on energetically non-uniform surfaces (Equation 8):

qt =β1 ln(αβ)+β1 lnt(8)

where qt is the adsorption capacity at time t(μg/cm²), qe is the equilibrium adsorption capacity (μg/cm²), k1 (h^{-1}) and k2 ($cm^2/(\mu g \cdot h)$) are rate constants for the pseudo-first-order and pseudo-second-order models, respectively, and α($\mu g/(cm^2 \cdot h)$) and β($cm^2/\mu g$) are Elovich constants related to initial adsorption rate and desorption constant, respectively. Model fits were evaluated using the coefficient of determination (R2).

3. Results and Discussion

3.1 Membrane Characterization

3.1.1 Morphological Analysis

SEM imaging revealed distinct structural features of the PES substrate and composite membranes (Figure 2). The pristine PES substrate exhibited a typical asymmetric structure with a dense top layer and interconnected finger-like pores extending to the bottom (Figure 2a,e). After coating with PDMS or HEMA-PDMS, the membrane surface became uniformly smooth and dense, with no visible defects such as pinholes or cracks (Figure 2b–d). Cross-sectional images confirmed that the coating layer formed a continuous, defect-free interface with the PES substrate, with no penetration of the coating solution into the underlying finger-like pores (Figure 2f,g). This intact interface is critical for preventing blood leakage and maintaining gas barrier properties in oxygenator applications. The thickness of the HEMA-PDMS functional layer increased marginally with higher coating solution concentrations (from ~1.2 μm for 2H-P/P to ~1.8 μm for 6H-P/P), consistent with previous reports on PDMS-based composite membranes [19].

DOI:

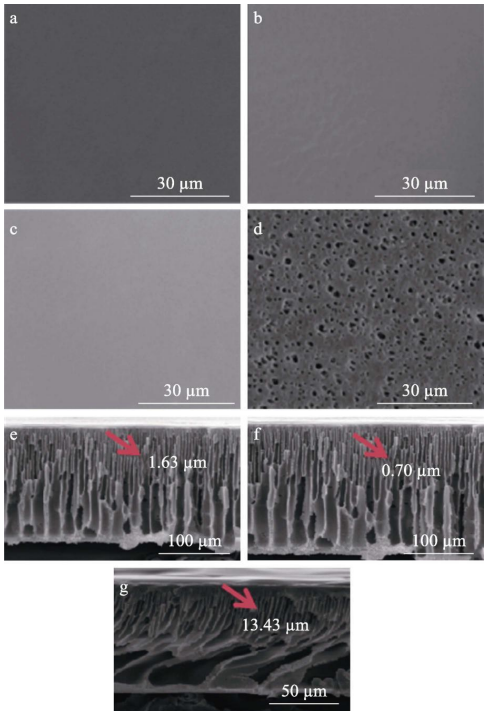

Figure 2 Surfaces (a~d) and sections (e~g) SEM images of different membranes

3.1.2 Chemical Structure Analysis

FTIR spectroscopy confirmed the successful copolymerization of HEMA and PDMS (Figure 3). The spectrum of pristine PDMS showed characteristic peaks at 2962 cm^{-1} (C–H stretching of $–CH_3$), 1260 cm^{-1} (Si–C stretching), and 1026 cm^{-1} (Si–O–Si asymmetric stretching), consistent with literature values [20]. In contrast, the HEMA-PDMS spectrum exhibited a new absorption peak at 1750 cm^{-1} corresponding to the C=O stretching vibration of the ester group (–COOR) in HEMA, which overlapped with the weakened C=C stretching peak of PDMS at 1640 cm^{-1}. This shift indicates successful grafting of HEMA onto PDMS via free radical copolymerization, where the vinyl groups of HEMA react with the pendant vinyl groups of PDMS. Importantly, the Si–C and Si–O–Si peaks of PDMS remained unchanged in HEMA-PDMS, confirming that copolymerization occurred exclusively on the side chains without disrupting the PDMS backbone—a key factor preserving the gas permeability of the copolymer.

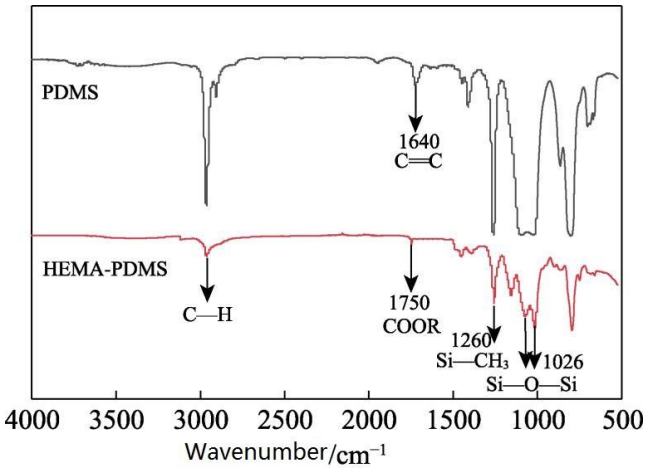

Figure 3 FTIR spectra of PDMS and HEMA-PDMS

3.1.3 Thermal Stability

TGA curves revealed excellent thermal stability of all composite membranes (Figure 4). Pristine PES began to degrade at ~450 °C, consistent with its aromatic backbone structure. Unmodified PDMS/PES membranes (2P/P) showed initial mass loss at ~500 °C, corresponding to the thermal decomposition of PDMS. In contrast, HEMA-PDMS/PES membranes (2H-P/P, 4H-P/P, 6H-P/P) exhibited no mass loss below 400 °C, with decomposition initiating at ~400 °C and completing by 600 °C. The slightly earlier degradation of HEMA-PDMS compared to pristine PDMS is attributed to the lower thermal stability of the HEMA segments. Crucially, all membranes maintained structural integrity up to 100 °C, far exceeding the physiological temperature (37 °C) required for ECMO operation, confirming their suitability for in vivo applications. The minimal difference in TGA profiles between composite membranes and PES reflects the low mass fraction of the HEMA-PDMS coating layer (~2–6 wt% of total membrane mass).

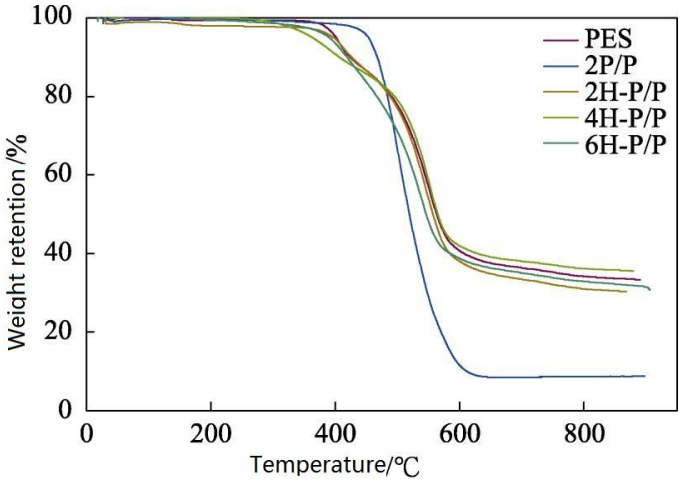

Figure 4 TGA curves of PES, 2P/P, 2H-P/P, 4H-P/P and 6H-P/P

3.1.4 Surface Hydrophilicity

Water contact angle (WCA) measurements quantified the impact of HEMA modification on surface hydrophilicity (Figure 5). Unmodified PDMS/PES membranes (2P/P, 4P/P, 6P/P) exhibited high WCAs of 105.97°, 103.14°, and 102.16°, respectively, consistent with the intrinsic hydrophobicity of PDMS. In stark contrast, HEMA-PDMS/PES membranes displayed significantly reduced WCAs of 40.43°, 40.22°, and 39.64° for 2H-P/P, 4H-P/P, and 6H-P/P, respectively—all within the hydrophilic range (<90°). Notably, WCA values were nearly identical across HEMA-PDMS membranes regardless of coating solution concentration (2–6 wt%), indicating that the surface composition was dominated by HEMA segments rather than PDMS. This phenomenon arises from the amphiphilic nature of HEMA-PDMS: during coating and curing, the hydrophobic PDMS segments preferentially orient toward the PES substrate, while the hydrophilic HEMA segments migrate to the aqueous interface, forming a stable, HEMA-enriched surface layer [21]. The consistent WCA confirms that this surface segregation occurs reproducibly across varying coating thicknesses, a desirable feature for scalable membrane fabrication.

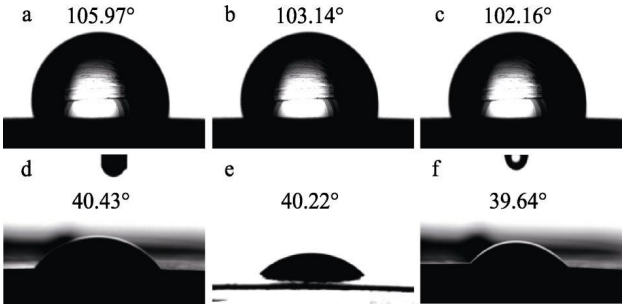

Figure 5 Water contact angle of composite membranes surface

3.2 Gas Permeation Performance

Gas permeation properties are paramount for oxygenator membranes, as they directly determine CO_2 removal and O_2 delivery efficiency. Figure 6 summarizes the CO_2 permeability and CO_2/O_2 selectivity of all composite membranes. For both PDMS/PES and HEMA-PDMS/PES series, CO_2 permeability decreased with increasing coating solution concentration (from 2 to 6 wt%). This trend is attributed to the thicker functional layer at higher coating concentrations, which increases the diffusion path length for gas molecules, thereby elevating mass transfer resistance. At equivalent coating concentrations, HEMA-PDMS/PES membranes exhibited lower CO_2 permeability than their PDMS/PES counterparts. Two factors contribute to this reduction: (1) HEMA segments introduce steric hindrance that restricts the mobility of PDMS chains, reducing free volume for gas diffusion; (2) HEMA-PDMS solutions have lower viscosity than pristine PDMS solutions, leading to partial penetration of the coating into PES pores and increased effective thickness of the dense layer.

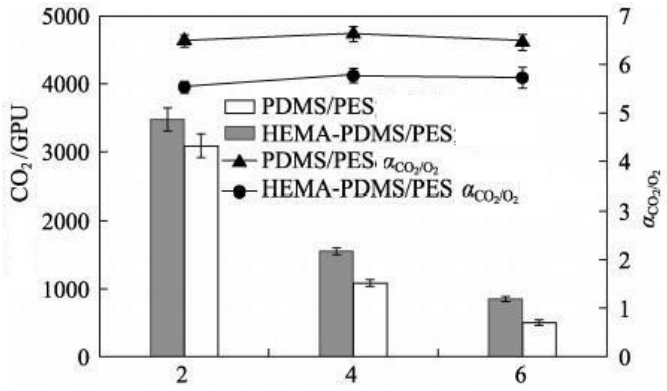

Figure 6 CO2 permeability and gas permeability selectivity of 2P/P, 4P/P, 6P/P, 2H-P/P, 4H-P/P and 6H-P/P

Despite lower absolute permeability, HEMA-PDMS/PES membranes demonstrated significantly higher CO_2/O_2 selectivity (6.53 for 4H-P/P) compared to PDMS/PES membranes (~5.2 for 4P/P). This enhancement is ascribed to the selective interaction between CO_2 and HEMA hydroxyl groups: CO_2, being a quadrupolar molecule, forms weak hydrogen bonds with the –OH groups of HEMA, increasing its solubility in the membrane matrix. In contrast, O_2 (nonpolar) exhibits minimal interaction with HEMA, relying solely on diffusivity for transport. The combination of reduced O_2 diffusivity (due to HEMA-induced chain stiffening) and enhanced CO_2 solubility results in improved selectivity—a critical advantage for ECMO, where efficient CO_2 removal is often more challenging than O_2 delivery [22]. Among HEMA-PDMS membranes, 4H-P/P offered the optimal balance between permeability and selectivity, making it the focus of subsequent hemocompatibility and protein adsorption studies.

3.3 Hemocompatibility Evaluation

Hemolysis rate serves as a primary indicator of erythrocyte compatibility for blood-contacting materials. According to ISO 10993-2017, biomedical materials must exhibit a hemolysis rate <5% to be deemed safe for clinical use. As shown in Figure 7, unmodified PDMS/PES membranes had hemolysis rates ranging from 0.521% to 0.668%, while HEMA-PDMS/PES membranes exhibited significantly lower values of 0.207%–0.434%—well below the 5% threshold. This improvement is attributed to the enhanced surface hydrophilicity of HEMA-PDMS: hydrophilic surfaces reduce interfacial tension between the membrane and blood, minimizing mechanical stress on erythrocytes and preventing membrane disruption [23]. Additionally, the hydration layer formed by HEMA-bound water molecules acts as a physical barrier, inhibiting direct contact between red blood cells and the hydrophobic PDMS backbone, further reducing hemolysis. The lowest hemolysis rate observed for 4H-P/P (0.207%) aligns with its optimal surface hydrophilicity (WCA ~40°), as excessively high hydrophilicity can also promote protein adsorption and complement activation [24]. These results confirm that HEMA modification effectively enhances the hemocompatibility of PDMS-based membranes, addressing a key limitation of conventional ECMO materials.

DOI:

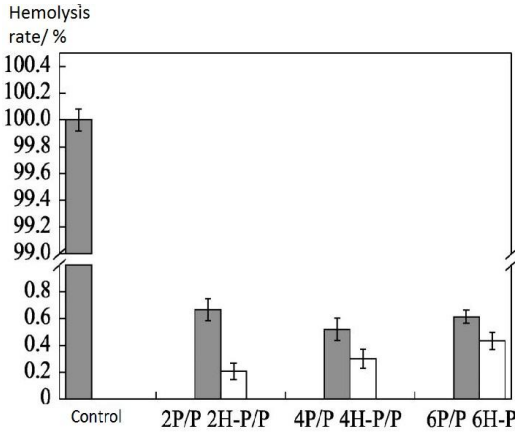

Figure 7 Hemolysis ratios of 2P/P, 4P/P, 6P/P, 2H-P/P, 4H-P/P and 6H-P/P

3.4 Protein Adsorption Behavior

3.4.1 Effect of BSA Concentration

Equilibrium adsorption isotherms reveal how BSA adsorption varies with bulk protein concentration (Figure 8). For all membranes, adsorption capacity increased with rising BSA concentration until reaching a plateau, indicative of monolayer coverage. Fitting the data to the Langmuir model (Table 1) yielded high correlation coefficients (R2>0.97), confirming that BSA adsorption follows monolayer chemisorption on a homogeneous surface. The maximum adsorption capacity (qm) decreased progressively with higher HEMA content: 2P/P (240.74 ± 2.37 μg/cm²) > 2H-P/P (227.23 ± 1.95 μg/cm²) > 4H-P/P (213.19 ± 1.41 μg/cm²) > 6H-P/P (208.25 ± 1.59 μg/cm²). Relative to unmodified 2P/P, HEMA modification reduced qm by 5.61%, 11.44%, and 13.49% for 2H-P/P, 4H-P/P, and 6H-P/P, respectively. This reduction is attributed to the hydration layer on HEMA-modified surfaces, which sterically hinders BSA access to adsorption sites. However, the relatively modest decrease in qm (vs. expectations for highly hydrophilic surfaces) suggests additional adsorption mechanisms beyond simple steric hindrance, as discussed later.

Table 1 Adsorption parameters of BSA at different mass concentrations by Langmuir model

Composite Membrane	Ka / (mL/μg)	qm / (μg/cm²)	R2
2P/P	(9.01±0.77)×10−3	240.73552±2.37139	0.97872
2H-P/P	(7.13±0.44)×10−3	227.22504±1.94811	0.98970
4H-P/P	(10.26±0.66)×10−3	213.19385±1.40738	0.98764
6H-P/P	(11.82±0.99)×10−3	208.25133±1.59223	0.97824

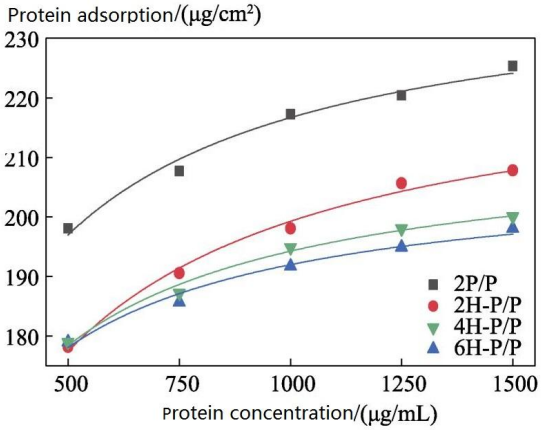

Figure 8 Adsorption capacity of BSA at different mass concentrations by 2P/P, 2H-P/P, 4H-P/P and 6H-P/P

3.4.2 Effect of Temperature

Temperature dependence of BSA adsorption provides insights into the thermodynamics of the process (Figure 9). From 27 to 37 °C (physiological range), adsorption capacity remained nearly constant for all membranes, indicating that temperature has negligible impact on protein adsorption under normal ECMO operating conditions. However, when temperature increased to 42 °C, adsorption dropped sharply for all membranes, with a more pronounced decline at 47 °C. This abrupt decrease is attributed to BSA denaturation: BSA maintains its native globular structure (three α-helices, 17 disulfide bonds) below 40 °C, but undergoes irreversible unfolding above its denaturation temperature (~42 °C) [25]. Denaturation exposes internal hydrophobic residues, disrupts polar group distribution, and reduces the ability of BSA to form hydrogen bonds with HEMA, leading to decreased adsorption. Notably, HEMA-PDMS membranes retained higher adsorption capacity than PES and PDMS/PES at elevated temperatures, likely due to residual hydrophobic interactions between PDMS and exposed nonpolar regions of denatured BSA. These results confirm that the composite membranes are stable and effective for protein resistance within the physiological temperature range relevant to ECMO.

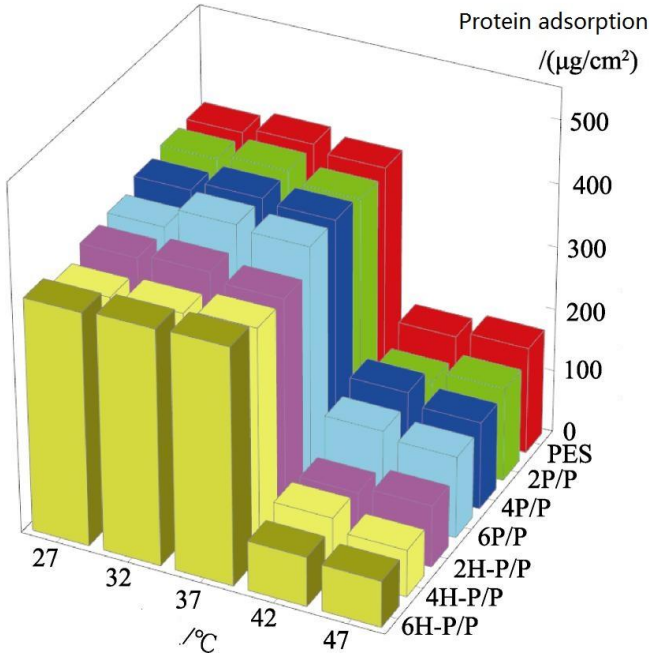

Figure 9 BSA adsorption capacity of PES, PDMS/PES composite membrane and HEMA-PDMS/PES composite membrane at different temperatures

3.4.3 Adsorption Kinetics

Kinetic analysis of BSA adsorption on 4H-P/P (Figure 10) reveals a rapid initial adsorption phase (0–2 h), followed by a slower approach to equilibrium (2–12 h), and saturation after 12 h. This biphasic behavior is typical of protein adsorption: the initial fast step corresponds to diffusion-controlled transport of BSA to the membrane surface, while the slower step reflects rearrangement of adsorbed proteins and occupation of remaining binding sites [26]. Fitting experimental data to three kinetic frameworks (Table 2) revealed inadequate performance of the Elovich model (R^2 = 0.806), indicating its unsuitability for describing the adsorption mechanism. Both the pseudo-first-order (R^2 = 0.984) and pseudo-second-order (R^2 = 0.997) models demonstrated satisfactory correlation, though the latter exhibited superior agreement with empirical observations, particularly at extended contact durations. The equilibrium adsorption capacity derived from the pseudo-second-order formalism (208.68 μg/cm²) closely concurred with the Langmuir maximum monolayer capacity (q = 213.19 μg/cm²), substantiating chemisorption as the predominant adsorption mechanism. This chemisorption is driven by hydrogen bonding between polar groups (–OH, $–NH_2$, –COOH) of BSA and the hydroxyl groups of HEMA, as well as potential electrostatic interactions at physiological pH (BSA has a net negative charge, while HEMA-PDMS surfaces are slightly negatively charged due to trace silanol groups) [27].

Table 2 Three kinetic model parameters of 4H-P/P for BSA adsorption

Pseudo-first-order kinetic model			Pseudo-second-order kinetic model			Elovich kinetic model		
Q0 / (μg/cm²)	k1 / h⁻¹	R2	Q0 / (μg/cm²)	k2 /[cm²/(μg·h)]	R2	α	β	R2
200.463	1.931	0.984	208.678	0.017	0.997	9.824×109	0.117	0.806

3.4.4 Adsorption Mechanism Discussion

While HEMA modification reduced BSA adsorption relative to unmodified PDMS, the decrease was less pronounced than expected for a fully hydrophilic surface. This discrepancy can be explained by the complex adsorption behavior of BSA, a large globular protein (66.5 kDa) with multiple interaction sites: (1) Competitive hydrogen bonding: BSA competes with water molecules for HEMA hydroxyl groups, and some BSA molecules adsorb by displacing water from the hydration layer, forming direct HEMA–BSA hydrogen bonds. (2) Secondary hydration layer adsorption: BSA polar groups can form hydrogen bonds with water molecules in the outer hydration layer, allowing adsorption without direct contact with HEMA. (3) Hydrophobic interactions: Upon initial adsorption, BSA may undergo minor conformational changes that expose internal hydrophobic patches, which interact with the underlying PDMS segments of the copolymer. These combined interactions—hydrogen bonding, hydration-mediated adsorption, and hydrophobic effects—result in measurable residual adsorption even on hydrophilic HEMA-PDMS surfaces. Nevertheless, the 11.44% reduction in qm for 4H-P/P translates to significantly lower protein surface coverage, which is sufficient to reduce platelet adhesion and thrombus formation in practical applications [28].

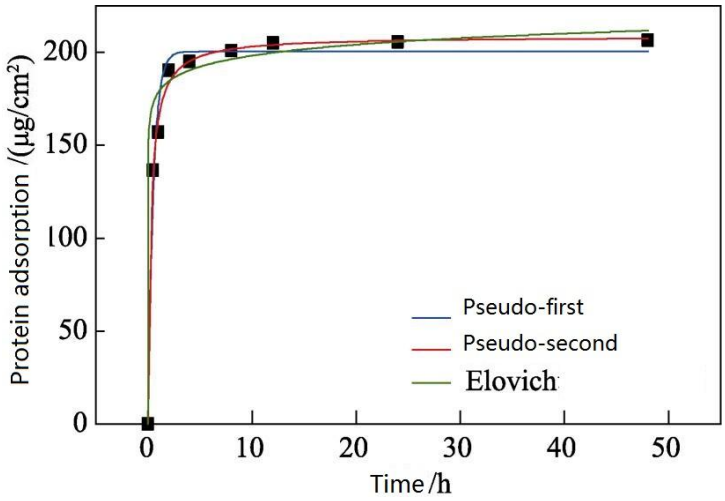

Figure 10 Kinetics fitting curves of 4H-P/P for BSA adsorption

4. Conclusions

This study successfully fabricated HEMA-PDMS/PES composite membranes via free radical copolymerization of HEMA and PDMS, followed by coating onto a porous PES substrate. Key findings include:

Structural and Thermal Properties: HEMA-PDMS formed a dense, defect-free functional layer on PES, with no mass loss below 400 °C, ensuring thermal stability for physiological applications. Surface hydrophilicity was dramatically enhanced (WCA ~40°) and independent of coating concentration due to surface segregation of HEMA segments.

Gas Separation Performance: The optimized 4H-P/P membrane achieved a CO_2/O_2 selectivity of 6.53, outperforming unmodified PDMS/PES membranes. This enhancement is attributed to selective CO_2–HEMA interactions, despite a slight reduction in absolute permeability due to increased diffusion resistance.

Hemocompatibility: HEMA modification reduced hemolysis rates to 0.207%–0.434% (vs. 0.521%–0.668% for

PDMS/PES), meeting ISO 10993-2017 standards. The hydration layer on HEMA surfaces minimized erythrocyte damage, a critical advantage for blood-contacting devices.

Protein Adsorption Mechanism: BSA adsorption followed the Langmuir isotherm and pseudo-second-order kinetic models, confirming chemisorption via hydrogen bonding between BSA polar groups and HEMA hydroxyls. Maximum BSA adsorption was reduced by up to 13.49% relative to unmodified PDMS/PES, with adsorption stable at physiological temperatures (27–37 °C) but decreasing sharply above 42 °C due to protein denaturation.

These results position HEMA-PDMS/PES composite membranes as promising candidates for next-generation ECMO oxygenators, offering a balanced combination of gas selectivity, hemocompatibility, and protein resistance. Future work will focus on in vitro whole-blood perfusion studies to validate antithrombogenic performance and explore long-term stability under simulated ECMO conditions. This research provides a theoretical foundation for designing advanced membrane materials to mitigate thrombotic complications in ECMO, ultimately improving patient outcomes in critical care settings.

References

[1] Sun T, Zhi L H, Cheng C, et al. Application of hydrophilic and low-surface-energy anti-fouling membrane for ECMO[J]. Journal of Membrane Science, 2022, 701: 122770.

[2] He T, He J H, Wang Z H, et al. Modification strategies to improve the membrane hemocompatibility in extracorporeal membrane oxygenator (ECMO)[J]. Advanced Composites and Hybrid Materials, 2021, 4: 847-864.

[3] He T, Yu S H, He J H, et al. Membranes for extracorporeal membrane oxygenator (ECMO): History, preparation, modification and mass transfer[J]. Chinese Journal of Chemical Engineering, 2022, 49: 46-75.

[4] Tie J, Zhang C L, Weng Y X. Research progress of membrane materials in extracorporeal membrane oxygenation system[J]. Membrane Science and Technology, 2020, 40(6): 141-147.

[5] Oguz O T, Aysegul D A, Seyed A N, et al. Polymeric hollow fiber membrane oxygenators as artificial lungs: A review[J]. Biochemical Engineering Journal, 2022, 180: 108440.

[6] Kalulu M, Oderinlo O, Wei Y Y, et al. Robust solvent-free fabrication and characterization of polydimethylsiloxane-co-2-hydroxyethylmethacrylate/poly(ethylene glycol) methacrylate (PDMS-HEMA)/PEGMA hydrogels[J]. Polymers for Advanced Technologies, 2019, 30(8): 1922-1932.

[7] Zhang X J, Zhang X L, Du B Y, et al. Amphiphilic PDMS-HEMA membrane surface for improved gas selectivity and blood compatibility[J]. Journal of Membrane Science, 2020, 690: 122183.

[8] Hanifi S, Farahmandghavi F, Imani M. RAFT-derived siloxane-based amphiphilic triblock copolymers: Synthesis, characterization, and self-assembly[J]. European Polymer Journal, 2020, 135: 109874.

[9] Farzad S, Zhao W F, Xiao H N, et al. Radical polymerization as a versatile tool for surface grafting of thin hydrogel films[J]. Polymer Chemistry, 2020, 11: 4355-4381.

[10] Zheng A R. Preparation of superhydrophobic surfaces and study of blood compatibility[D]. Zhenjiang: Jiangsu University, 2007.

[11] Dong X. Summary of blood compatibility materials[J]. Journal of Qingdao University, 2000, 15(4): 32-35.

[12] Tu M M, Xu J J, Qiu Y R. Surface hemocompatible modification of polysulfone membrane via covalently grafting acrylic acid and sulfonated hydroxypropyl chitosan[J]. RSC Advances, 2019, 9(11): 6254-6266.

[13] Zheng L, Wang H S, Ouyang Y F, et al. Preparation of plasma-initiated SMCC grafted polystyrene microplate and its adsorption properties for protein[J]. Fine Chemicals, 2021, 38(6): 1141-1146

[14] Liu H L, Li J D, Li H Y, et al. Constitution of the micro-nano structure of APDMS-MMT/SiO_2 RTV-1 and superhydrophobic study[J]. New Chemical Materials, 2017, 45(7): 87-89

[15] Wei J F, Liu X X, Jia K L, et al. Construction of dual-functional coating of biomimetic phospholipid polymer and silver nanoparticles and its antifouling and antibacterial properties[J]. Fine Chemicals, 2021, 42(4): 828-836, 928

[16] Yang M. Study on adsorption capacity of carbon nanotubes to bovine serum albumin[D]. Yinchuan: Ningxia University, 2021.

[17] Wang Y N. Study on thermal stability and content detection of α-lactalbumin by differential scanning fluorescence[D]. Xi'an: Shaanxi University of Science & Technology, 2021.

[18] Zuo S, Chang J D, Liu M. Study on adsorption kinetics of HCl on the surface of ethanol-modified calcium adsorbent[J]. Power Equipment, 2020, 39(2): 71-78.
[19] Mostafa S, Majid T, Davood G. Adsorption of uranium(VI) from sulphate solutions using Amberlite IRA-402 resin: Equilibrium, kinetics and thermodynamics study[J]. Annals of Nuclear Energy, 2015, 75: 132-138.
[20] Robert A L. Fundamental principles of the thermodynamics and kinetics of protein adsorption to material surfaces[J]. Colloids and Surfaces B: Biointerfaces, 2020, 191: 110992.
[21] Matthew C, Aeryne L, Thanh P H, et al. Protein adsorption on blood-contacting surfaces: A thermodynamic perspective to guide the design of antithrombogenic polymer coatings[J]. Acta Biomaterialia, 2020, 180: 46-60.
[22] Zhang X J, Zhang X L, Du B Y, et al. Gas transport mechanisms in PDMS-based membranes for CO_2 separation[J]. Journal of Membrane Science, 2022, 654: 120542.
[23] Ratner B D, Hoffman A S, Schoen F J, et al. Biomaterials Science: An Introduction to Materials in Medicine[M]. 4th ed. Amsterdam: Elsevier, 2020: 345-367.
[24] Shen M, García I, Maier R V, et al. Effects of surface chemistry on complement activation by polymeric biomaterials[J]. Journal of Biomedical Materials Research Part A, 2006, 78A(1): 163-174.
[25] Bhattacharjee C, Das K P. Thermal unfolding of bovine serum albumin: A spectroscopic and calorimetric study[J]. International Journal of Biological Macromolecules, 2000, 27(4): 321-328.
[26] Norde W. Adsorption of proteins from solution at the solid-liquid interface[J]. Advances in Colloid and Interface Science, 1986, 25(4): 267-340.
[27] Rahaman M S, Théato P. Surface modification of polymers for biomedical applications: Mechanisms and applications[M]//Surface Modification of Polymers. Berlin: Springer, 2019: 1-32.
[28] Gorbet M B, Sefton M V. Biomaterial-associated thrombosis: Roles of coagulation factors, complement, platelets and leukocytes[J]. Biomaterials, 2004, 25(26): 5681-5703.